THE JOURNAL OF PHYSICAL CHEMISTRY C

pubs.acs.org/JPCC

Article

NMR and Raman Scattering Studies of Temperature- and Pressure-Driven Phase Transitions in $CH_3NH_2NH_2PbCl_3$ Perovskite

Mirosław Mączka,* Maciej Ptak, Daniel Linhares Militão Vasconcelos, Laisvydas Giriunas, Paulo Tarso Cavalcante Freire, Marko Bertmer, Juras Banys, and Mantas Simenas

Cite This: *J. Phys. Chem. C* 2020, 124, 26999−27008

Read Online

ACCESS | Metrics & More | Article Recommendations | Supporting Information

ABSTRACT: Three-dimensional methylhydrazinium ($CH_3NH_2NH_2^+$, MHy^+) lead halides, related to the famous methylammonium ($CH_3NH_3^+$, MA^+) and formamidinium ($CH(NH_2)_2^+$, FA) perovskites, are attractive optoelectronic materials crystallizing in polar structures. In this work, temperature-dependent ^1H and ^{207}Pb magic-angle spinning (MAS) NMR, Raman as well as high-pressure Raman studies of $CH_3NH_2NH_2PbCl_3$ ($MHyPbCl_3$) are reported. Raman spectroscopy reveals many similarities between phonon properties of MHy lead halides and the MA and FA analogues. In particular, these families of compounds show an increase in wavenumber of cage modes when large I^- ions are replaced by smaller Br^- and then Cl^- ones. They also show strong sensitivity of the CH_3 torsional mode on size of the cavity occupied by MHy^+ cation that decreases with decreasing size of the halide anion. The cage modes of $MHyPbCl_3$ are, however, observed at significantly lower wavenumbers than similar modes of $MAPbCl_3$ and $FAPbCl_3$, indicating higher softness of $MHyPbCl_3$. Temperature-dependent Raman and NMR studies demonstrate that the MHy^+ cations in $MHyPbCl_3$ are significantly less affected by the temperature-induced phase transition than the Pb−Cl framework. This suggests a displacive type of the phase transition dominated by tilting and deformation of the $PbCl_6$ octahedra. Analysis of the ^{207}Pb MAS NMR spectra reveals the presence of two differently distorted $PbCl_6$ octahedra and diminishing (increasing) distortion of the less (more) distorted octahedra in the high-temperature phase. Pressure-dependent Raman studies reveal the presence of a single first-order pressure-induced phase transition between 0.72 and 1.27 GPa. Analysis of the spectra indicates that the driving forces for the pressure-induced phase transition in $MHyPbCl_3$ are tilting and distortion of the $PbCl_6$ octahedra accompanied by reorientation of MHy^+ cations. Raman spectra do not show evidence of any additional phase transition or amorphization up to 6.95 GPa.

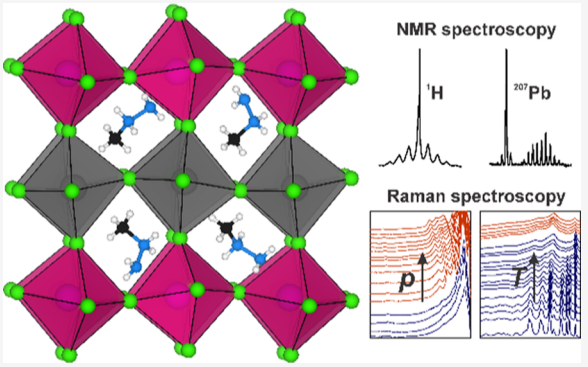

INTRODUCTION

Perovskite-type hybrid organic−inorganic compounds are very important functional materials.[1,2] For instance, formates are known for their multiferroic properties,[3−7] while dicyanamides and cyanides are promising barocaloric and dielectric switchable materials.[8−13] The most famous group of perovskite-type compounds are, however, metal halides.[14−23] In particular, three-dimensional (3D) ABX_3 halides (A = MA^+, FA^+, or Cs^+ cation; B = Pb^{2+}, Sn^{2+}, Ge^{2+}; X = Cl^-, Br^-, I^-) are very important optoelectronic materials exhibiting remarkable photovoltaic and photoluminescent (PL) properties as well as strong multiphoton absorption, making them suitable for applications in solar cells, light-emitting devices, photodetectors, and scintillators, among others.[17−23] Very recently, we have discovered that 3D perovskites may also be constructed using MHy^+ cations.[24,25] Similarly to their famous formamidinium (FA) and methylammonium (MA) analogues, $MHyPbBr_3$ and $MHyPbCl_3$ compounds also demonstrated PL properties.[24,25] Furthermore, $MHyPbBr_3$ showed very strong two-photon absorption and switchable dielectric properties.[24] However, in contrast to the FA and MA lead halides, MHy analogues crystallize in polar structures and exhibit significant second-harmonic generation (SHG) activity.[24,25] It is also worth to add that $MHyPbCl_3$ demonstrates unprecedented quadratic nonlinear optical (NLO) switching in which SHG response was switched between the room-temperature (RT) low-SHG state and the high-temperature (HT) high-SHG state.[25]

Properties of hybrid perovskites are very often strongly affected by structural changes occurring due to structural phase transitions associated with deformation of the framework and ordering−disordering of organic cations.[3,7−13,16,24−26] Such structural changes may, for instance, lead to onset of polar

Received: August 29, 2020
Revised: October 15, 2020
Published: November 24, 2020

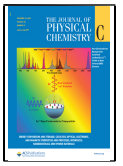

order,[3,7] sudden change of dielectric permittivity,[10−13,16] or appearance of second-order NLO properties.[10,24,25] It is, therefore, of great importance to understand the mechanism behind these structural changes. Our previous X-ray diffraction (XRD) studies showed that the HT phase of $MHyPbBr_3$ is isostructural to the HT phases of FA and MA, i.e., these phases adopt the cubic space group $Pm\bar{3}m$ with disordered organic cations.[24] On cooling, $MHyPbBr_3$ transforms into the ordered low-temperature (LT) monoclinic phase (space group $P2_1$) at 409 K.[24] $MHyPbCl_3$ adopts the same polar space group $P2_1$ at RT, but on heating, it undergoes a temperature-induced phase transition at 342 K to the HT orthorhombic structure (space group $Pb2_1m$) with ordered MHy^+ cations (see Figure 1).[25] X-

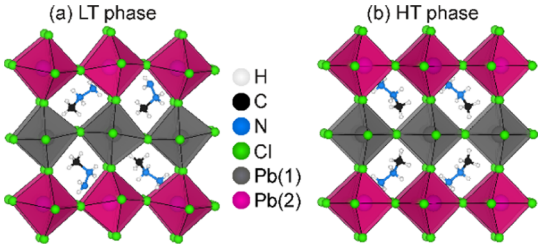

Figure 1. Crystal structure of $MHyPbCl_3$ in the (a) LT and (b) HT phases. Data are taken from ref 25.

ray diffraction and dielectric spectroscopy relate this transition to a tilt of $PbCl_6$ octahedra and reorientation of MHy^+ cations.[25] However, the mechanism of this phase transition is still obscured and there is need for other experimental studies using methods that are sensitive for local structural changes. A well-known and very sensitive method to probe structural changes is Raman spectroscopy that was successfully employed in studies of various organic−inorganic hybrid perovskites, including lead halides.[7,11,13,24,25,27,28] Another powerful method to study the structural phase transitions in various compounds is nuclear magnetic resonance (NMR) spectroscopy.[29] This technique has been widely used to investigate transition phenomena in metal-formate frameworks[30−32] and lead halide perovskites.[33−40] In lead halide perovskites, NMR spectroscopy has been mostly used to study the structural changes of the PbX_6 octahedra[37,39] and the dynamics of the organic cations.[33,35−41] Previous NMR studies of $CsPbX_3$[33,36] and $MAPbX_3$ have convincingly shown that the dynamics of Cs^+ and MA^+ cations in lead halides change drastically during phase transitions.[33,35−40] In these materials, the most studied isotopes are ^1H, ^{13}C, and ^{207}Pb, which have a nuclear spin I = 1/2. The structural phase transitions and cation dynamics in these compounds are usually investigated by performing static[36,37,39] and magic-angle spinning (MAS)[37−40] experiments and longitudinal relaxation time measurements.[33,35,36,40,41]

In addition to temperature, pressure is another important thermodynamic parameter that strongly affects structural and thus physicochemical properties of materials. The effect of pressure on 3D lead halide perovskites has been studied both for MA and FA lead halides.[42−49] High-pressure diffraction and Raman studies of $MAPbX_3$ (X = Cl, Br, I) and $FAPbX_3$ (X = Br, I) showed that these perovskites usually exhibit two phase transitions, one below 1 GPa and another one in the 1.6−2.8 GPa range.[42−49] The lower pressure transitions were shown to be related with tilts and distortion of the PbX_6 octahedral units.[42−48] The mechanism of the higher-pressure phase transitions is less clear, but some papers suggested ordering of the organic cations as a possible driving force.[45] It is also worth to add that a few reports suggested pressure-induced amorphization, observed usually above 5 GPa.[45,46]

In this work, we report a combined Raman as well as ^1H and ^{207}Pb MAS NMR study of $MHyPbCl_3$ to obtain deeper insight into the structural changes of the lead-chloride framework and the dynamics of the MHy^+ cations during the phase transition. We also performed high-pressure Raman measurements to obtain information on stability of this material under compression. We show that $MHyPbCl_3$ undergoes a pressure-induced phase transition that is associated with a significant change of the lead halide framework.

EXPERIMENTAL SECTION

Synthesis. $MHyPbCl_3$ crystals were grown using the antisolvent method as described in detail in a previous publication.[25]

Temperature-Dependent Raman. Raman spectra were measured for a single crystal using a Renishaw InVia Raman spectrometer equipped with a confocal DM 2500 Leica optical microscope, a thermoelectrically cooled charged coupled device (CCD) as detector, and an argon laser (λ_{exc} = 488 nm). To obtain information on low-wavenumber optical modes, additional measurements were performed using the same instrument, an eclipse filter, and a diode laser (λ_{exc} = 830 nm). The temperature was controlled using a Linkam cryostat cell. The spectral resolution was 2 cm^{-1}.

Temperature-Dependent NMR. The ^1H NMR and longitudinal relaxation time T_1 measurements of $MHyPbCl_3$ were performed at a magnetic field strength of 9.4 T using a 400 MHz Bruker Avance 400 spectrometer. A 4 mm MAS probe was used with a spinning frequency of 9 kHz and a $\pi/2$ pulse length of 7.5 μs. The saturation recovery technique was used to measure the T_1 relaxation time.[50] The MAS spectra were referenced to the ^1H chemical shift of tetramethylsilane (TMS) using poly(dimethylsiloxane) (PDMS) as secondary reference (0.07 ppm). The ^{207}Pb NMR spectra of $MHyPbCl_3$ were acquired at 9.4 T using a Bruker Advance III HD spectrometer. A 4 mm double-resonance MAS probe at a frequency of 83.72 MHz was used with a $\pi/2$ pulse length of 3 μs. To measure the ^{207}Pb chemical shift tensor accurately, the MAS spectra were acquired at two different spinning frequencies (8 and 10 kHz). A total of 1024 scans were accumulated to ensure a sufficient signal-to-noise ratio. Chemical shifts δ were referenced to $Pb(CH_3)_4$ at 0 ppm using a 0.5 M aqueous $Pb(NO_3)_2$ solution as a secondary reference (δ = −2941 ppm vs $Pb(CH_3)_4$).[51] The deconvolution of the ^{207}Pb NMR spectra was performed using the DMfit software.[52] The measured temperature was calibrated based on the known phase-transition temperature of $MHyPbCl_3$.[25]

High-Pressure Raman Spectra. High-pressure Raman spectra were recorded with a LabRam HR spectrometer from Horiba with a CCD cooled with liquid nitrogen. The 632 nm line from a He−Ne laser was used as an excitation source. High pressure was obtained through a membrane diamond anvil cell equipped with stainless steel gaskets with holes of about 150 μm serving as the sample chamber and paraffin oil (Nujol) as the pressure-transmitting medium. To measure the pressure, we used the luminescence lines of chromium in small balls of ruby placed in the same hole in the gasket as the sample.

https://dx.doi.org/10.1021/acs.jpcc.0c07886
J. Phys. Chem. C 2020, 124, 26999−27008

RESULTS AND DISCUSSION

^{1}H NMR. To probe the local proton environment and MHy^+ cation dynamics during the phase transition, we performed ^{1}H MAS NMR measurements of the $MHyPbCl_3$ powder sample. The temperature-dependent ^{1}H NMR spectra are presented in Figure S1a,b.

The spectra show a single isotropic line with a chemical shift of about 3 ppm and spinning sidebands separated by 9 kHz. Unfortunately, the MAS frequency of 9 kHz was not sufficient to separate proton lines originating from two different proton environments of methyl and hydrazine. The 3 ppm value of the isotropic chemical shift is close to that of the methyl group in $MAPbX_3$ perovskites (3.4 ppm) and hydrazine (N_2H_4) (3.2 ppm).[38,39,53]

On heating above the phase-transition temperature, no substantial changes can be identified in the proton spectra and chemical shift value. In the related $MAPbX_3$ compounds, a significant change of the linewidth of the ^{1}H NMR signal is observed at the phase-transition points,[39] which is related to the pronounced order−disorder dynamics of the MA^+ cations. Our results indicate that such cation dynamics are absent in $MHyPbCl_3$ in agreement with the XRD results,[25] which show that long-range order of the MHy^+ cations is established in both structural phases of this compound.

To further study the cation dynamics in the vicinity of the phase transition, we also measured the temperature dependence of the ^{1}H longitudinal relaxation time T_1. The obtained dependence is presented in Figure 2, revealing an increase of

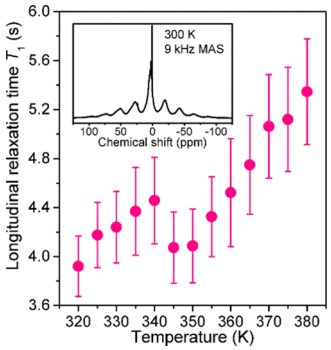

Figure 2. Temperature dependence of the ^{1}H longitudinal relaxation time T_1 of $MHyPbCl_3$. The inset presents a ^{1}H MAS NMR spectrum measured at 300 K.

T_1 on heating, while at the phase-transition point, a rather weak anomalous dip of T_1 is observed. Previous NMR studies of the related $MAPbX_3$ compounds revealed a much stronger decrease of T_1 at the phase-transition points,[35,38,39,41] indicating a significant role of the MA^+ cations in the phase-transition mechanism. In line with the analysis of the temperature-dependent ^{1}H spectra and previous XRD study,[25] our T_1 measurements reveal that the reorientation of the MHy^+ cations during the phase transition is not the phase transition driving mechanism in $MHyPbCl_3$.

^{207}Pb NMR. The XRD data revealed that the crystal structure of $MHyPbCl_3$ consists of two types of differently deformed $PbCl_6$ octahedra, namely, moderately distorted $Pb(1)Cl_6$ and significantly distorted $Pb(2)Cl_6$ (see Figure 1).[25] To study how these structural units are affected by the phase transition, we performed temperature-dependent ^{207}Pb MAS NMR measurements. The obtained spectra are presented in Figure S1c, revealing two ^{207}Pb signals with substantially different chemical shift anisotropy. The signal with an isotropic chemical shift $\delta_{iso} = -711$ ppm at RT has a smaller anisotropy, and thus, it is assigned to the less distorted $Pb(1)Cl_6$ octahedra. The signal with $\delta_{iso} = -1680$ ppm at RT is assigned to the significantly more distorted $Pb(2)Cl_6$ octahedra. The integrated signal intensity is 1:1 in agreement with the XRD data.

^{207}Pb NMR studies performed at RT of the closely related $CsPbCl_3$ and $MAPbCl_3$ perovskites reported isotropic chemical shifts δ_{iso} of −728 and −646 ppm, respectively.[40,54,55] Note that these compounds contain uniformly deformed $PbCl_6$ octahedra.[56,57] These values are similar to $\delta_{iso} = -711$ ppm observed for the $Pb(1)Cl_6$ signal of $MHyPbCl_3$. A much higher chemical shift value of $Pb(2)Cl_6$ octahedra likely originates from a strong interaction with nitrogen of MHy^+ cation (see Figure 2 in ref 25).

Upon heating, a change of the chemical shift and lineshape of the broader ^{207}Pb MAS NMR spectrum is observed at around 345 K (Figure S1c), which can be related to the change of the distortion of the octahedra at the phase transition.[25] The temperature dependence of the isotropic chemical shift δ_{iso} for both lead sites is presented in Figure 3, indicating an overall

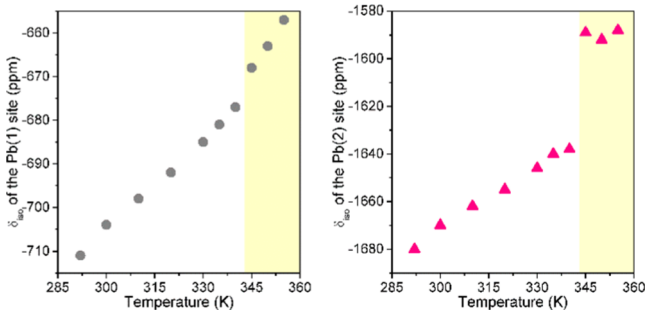

Figure 3. Temperature dependence of the isotropic chemical shift of ^{207}Pb(1) and ^{207}Pb(2) NMR signals of $MHyPbCl_3$.

decrease of δ_{iso} with decreasing temperature in agreement with other studies on related compounds.[37,39,40,54,55] Upon heating, at about 345 K, the chemical shift of both Pb(1) and Pb(2) NMR signals exhibits an anomalous increase, which is much more pronounced for the Pb(2) lead site (see Figure 3).

To further characterize the phase transition, we performed a deconvolution of the chemical shift tensor parameters based on the spinning sideband intensities of the experimental ^{207}Pb MAS NMR spectra.[52] Each deconvoluted spectrum of a single lead site is described by the chemical shift tensor δ, which, in the principal axis system, is expressed as[58]

$$\delta = \begin{pmatrix} \delta_{11} & 0 & 0 \\ 0 & \delta_{22} & 0 \\ 0 & 0 & \delta_{33} \end{pmatrix}$$

where $\delta_{33} > \delta_{22} > \delta_{11}$. The aforementioned isotropic chemical shift is $\delta_{iso} = 1/3\ (\delta_{11} + \delta_{22} + \delta_{33})_{33}$, while the anisotropy of the chemical shift tensor is frequently defined by the span and skew parameters.[58] The span parameter $\Omega = \delta_{33} - \delta_{11} > 0$ measures the maximum linewidth of the powder signal and defines the size of the anisotropy. The skew parameter $\kappa = (\delta_{22} - \delta_{iso})/\Omega$ defines the asymmetry of the δ tensor and can vary from −1 to +1. For $\kappa = 0$, $\delta_{22} = \delta_{iso}$, and for $\kappa = \pm 1$, δ_{22} is equal

https://dx.doi.org/10.1021/acs.jpcc.0c07886
J. Phys. Chem. C 2020, 124, 26999−27008

to either δ_{11} or δ_{33}.[58] In this study, we relate Ω and κ parameters to the distortion of the $PbCl_6$ octahedra in $MHyPbCl_3$.

The deconvoluted and experimental ^{207}Pb MAS NMR spectra obtained at 292 K (LT phase) and 350 K (HT phase) are presented in Figures S2 and S3 for 10 and 8 kHz MAS frequency, respectively. The deconvolution was performed with two different sets of parameters—one set for each Pb site. Using the same parameters to deconvolute the spectra obtained with different MAS rates increases the accuracy of the fit. The obtained δ_{iso}, Ω, and κ parameters for both types of $PbCl_6$ octahedra are presented in Table 1. They confirm that

Table 1. ^{207}Pb NMR Parameters of Pb(1) and Pb(2) Sites Determined at 292 and 350 K

T (K)	Pb site	δ_{iso} (ppm)	Ω (ppm)	κ
292	Pb(1)	−711(2)	241(5)	−0.18(1)
	Pb(2)	−1680(2)	931(6)	−0.16(1)
350	Pb(1)	−663(2)	198(6)	0.21(1)
	Pb(2)	−1592(2)	1039(7)	−0.09(1)

the $Pb(2)Cl_6$ octahedra are more distorted than the $Pb(1)Cl_6$ octahedra, but the degree of distortion is different in both structural phases of $MHyPbCl_3$. Distortion of the $Pb(1)Cl_6$ octahedra is larger in the LT phase than in the HT phase, while an opposite behavior is observed for the $Pb(2)Cl_6$ units. These results are in agreement with the behavior of the Pb−Cl bond length distortion Δd parameter, which shows an average octahedral distortion, measured in our previous X-ray diffraction study.[25]

To investigate the structural deformation at the phase transition point, we also analyzed the ^{207}Pb NMR spectra measured at the intermediate temperatures (not shown). The obtained temperature dependences of the Ω and κ parameters are presented in Figures 4 and S4, respectively. Both

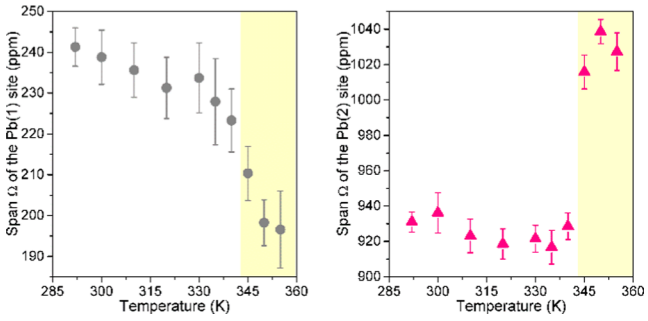

Figure 4. Temperature dependence of the span Ω parameter of ^{207}Pb(1) and ^{207}Pb(2) NMR signals of $MHyPbCl_3$.

parameters exhibit anomalous changes at the phase-transition point. Namely, upon heating, the span parameter of the $Pb(1)Cl_6$ octahedra decreases rather gradually, which may indicate a continuous character of the phase transition. However, the same parameter of the $Pb(2)Cl_6$ units shows a sudden increase characteristic to the first-order phase transition in agreement with the differential scanning calorimetry (DSC) results.[25]

Temperature-Dependent Raman. The crystal structure of $MHyPbCl_3$ is composed of corner-sharing $PbCl_6$ octahedra and MHy^+ cations located in the cavities of the framework.[25] Vibrational modes can be therefore subdivided into internal vibrations of MHy^+, lattice (translational and librational) modes of MHy^+, and vibrations of the Pb−Cl framework. There are 24 expected internal modes for a free MHy^+ cation, namely, 12 related to the NH_2 groups (symmetric stretching ($2\nu_s NH_2$), antisymmetric stretching ($2\nu_{as} NH_2$), scissoring ($2\delta NH_2$), rocking ($2\rho NH_2$), wagging ($2\omega NH_2$), torsion ($2\tau NH_2$)), three modes of the CNN skeletal group (symmetric stretching (ν_sCNN), antisymmetric stretching (ν_{as}CNN), and bending (δCNN)), and nine modes of the CH_3 groups (symmetric stretching ($\nu_s CH_3$), antisymmetric stretching ($2\nu_{as} CH_3$), symmetric bending ($\delta_s CH_3$), antisymmetric bending ($2\delta_{as} CH_3$), rocking ($2\rho CH_3$), and torsion (τCH_3)). Since the crystal structures of both HT phase (space group $Pb2_1m$) and LT phase (space group $P2_1$) comprise four formula units,[25] the total number of internal modes should increase to 96 (see the correlation diagram presented in Table S1). MHy^+ cations should also contribute to 12 translational and 12 librational modes. Regarding the Pb−Cl framework, there should be 48 such modes (Table S1). All internal and lattice modes should be Raman-active.

Temperature-dependent Raman spectra are shown in Figures 5 and S5−S8. The observed Raman modes and their

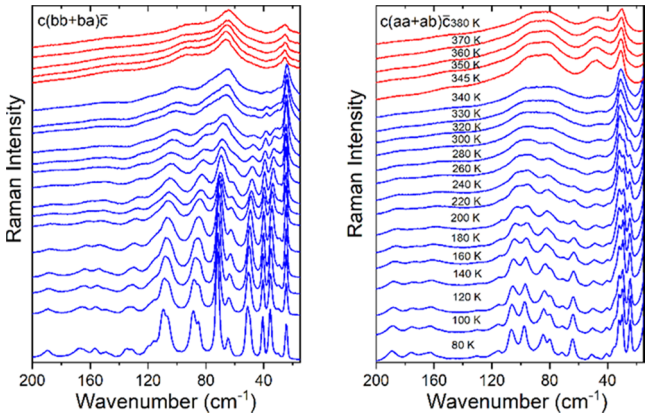

Figure 5. Temperature-dependent Raman spectra of $MHyPbCl_3$ in the 200−15 cm^{-1} range for c(bb + ba)c̄ and c(aa + ab)c̄ polarization configurations in heating run from 80 to 380 K.

assignment are listed in Table S2. Based on the Raman studies of methylhydrazinium metal formates[7] and lead halide perovskites,[16,24,25,27,28,59] all bands observed above 420 cm^{-1} can be attributed to pure internal modes of MHy^+ cations. Assignment of these modes to respective motion of atoms is proposed based on our previous studies of methylhydrazinium metal formates and $MHyPbBr_3$ as well as Raman and IR studies of methylhydrazine.[7,24,60] It is worth adding here that one band experiences a very pronounced shift when Br^- is replaced by Cl^-. This band, which shifts from 311 cm^{-1} for $MHyPbBr_3$ to 485 cm^{-1} for $MHyPbCl_3$, corresponds to the $\tau(CH_3)$ mode.[24] Former studies of $MAPbX_3$ perovskites also showed that the torsional mode exhibited large blue shift when I was replaced by smaller Br or Cl.[59] This behavior was attributed to strong coupling of the molecular torsion with the cage. Thus, the unusually large sensitivity of this mode to the halide atom seems to be a common feature of MHy- and MA-based perovskites.

Studies of isolated methylhydrazine molecules showed the presence of three N−H stretching modes at 3366, 3358, and 3314 cm^{-1}.[60] RT Raman spectra of $MHyPbCl_3$ show the

https://dx.doi.org/10.1021/acs.jpcc.0c07886
J. Phys. Chem. C 2020, 124, 26999−27008

presence of a doublet at 3286 + 3278 cm^{-1} and bands around 3223, 3170, 3150, and 3080 cm^{-1} (Figures S5 and S7). As can be seen, the N−H stretching bands of $MHyPbCl_3$ are significantly red-shifted, indicating the formation of medium-strength hydrogen bonds (HBs). It is worth to add that the N−H stretching modes of methylhydrazinium metal formates were observed in the 3320−2923 cm^{-1} range.[7] This behavior indicates that some N−H bonds form stronger HBs in the formates than in $MHyPbCl_3$.

Let us now discuss assignment of lattice modes. Former experimental (at 100 K) and density functional theory (DFT) studies performed for $MAPbX_3$ perovskites showed that the octahedra twist (librations) modes are observed at 26 and 32 cm^{-1} for the iodide, but they shift to higher wavenumbers for the bromide (to 39 and 47 cm^{-1}) and the chloride (to 42, 54 and 61 cm^{-1}).[59] The distortion (bending) modes were located at 42 + 47, 58, and 75 cm^{-1} for the I, Br, and Cl analogues, respectively. Increase of wavenumbers when Br is replaced by Cl was also observed for FA analogues.[28] RT Raman spectra of $MHyPbCl_3$ show the presence of intense bands at 24 and 32 cm^{-1} and a few weaker bands in the 46−29 cm^{-1} range (Figure 5). We assign these bands to the octahedra librations. The remaining intense bands, observed at RT in the 102−66 cm^{-1} range, can be most likely attributed to the bending modes. It is worth noting that for $MHyPbBr_3$, the intense bands corresponding to librational (bending) modes were observed at 22 and 18 cm^{-1} (69 and 45 cm^{-1}),[24] i.e., similarly to the MA and FA analogues, these modes shift to higher wavenumbers when Br^- is replaced by Cl^-. DFT and experimental studies of $MAPbX_3$ perovskites also revealed that remaining lattice modes, observed for $MAPbCl_3$ in the 238−94 cm^{-1} range (values at 100 K), show various degree of coupling between the cage modes (mainly Pb−X stretching) and organic cation modes (translations and librations).[59] We attribute to these modes Raman bands of $MHyPbCl_3$ in the 263−115 cm^{-1} range (values at 80 K).

Having discussed assignment of modes, we now move to discussion of temperature-dependent Raman spectra. To better visualize temperature changes in the Raman spectra, we show temperature dependence of wavenumbers and full width at half-maximum (FWHM) for several selected internal modes of MHy^+ cation (Figures 6 and 7). In the 340−80 K range,

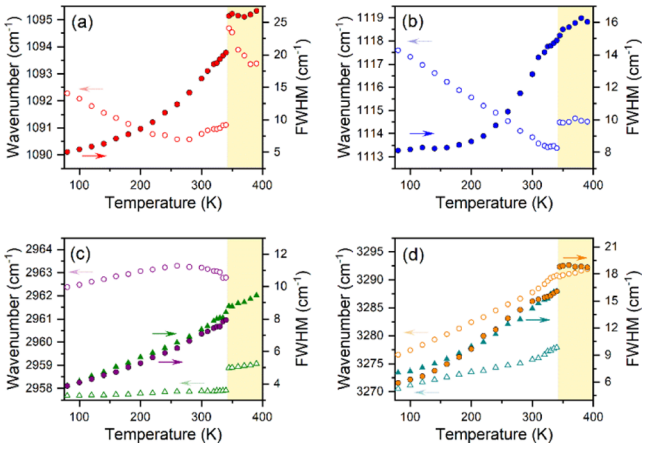

Figure 6. Temperature dependence of wavenumbers (open symbols) and FWHM (closed symbols) for several modes observed in the c(bb + ba)$\bar{c}$ polarization.

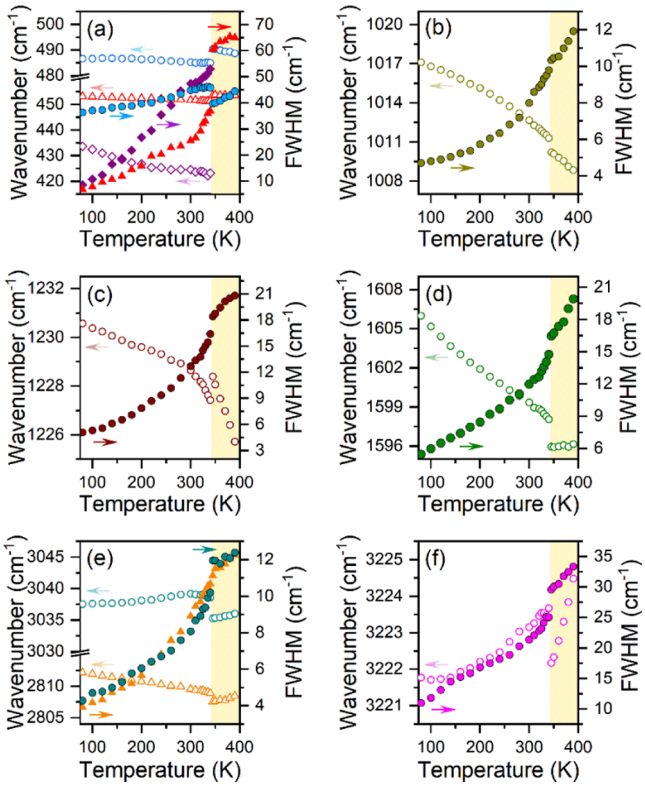

Figure 7. Temperature dependence of wavenumbers (open symbols) and FWHM (closed symbols) for several modes observed in the c(aa + ab)$\bar{c}$ polarization.

majority of these high-wavenumber modes exhibit usual blue shift on cooling, up to a few cm^{-1}. Opposite behavior is, however, observed for the 3288, 3276, and 3223 cm^{-1} modes assigned to the $\nu(NH_2)$ vibrations (Figures 6d and 7f). Red shift of these modes points to increased HB strength on cooling. Nearly all Raman bands related to internal modes show significant narrowing on cooling and FWHM values are typically below 10 cm^{-1} at 80 K (Figures 6, 7, and S5−S8). The only exception is the $\tau(CH_3)$ mode for which FWHM is 45.8 cm^{-1} at 340 K and 36.3 cm^{-1} at 80 K (Figure 7a). Similar narrowing of internal modes and a weak change of the FWHM for the CH_3 torsional mode were also reported for $MAPbX_3$ compounds, although $MAPbCl_3$ showed much weaker narrowing than its iodide and bromide analogues.[59]

In contrast to a relatively weak temperature dependence of MHy^+ internal modes, the lattice modes show much more pronounced changes. First of all, only a few broad bands are observed below 300 cm^{-1} at 340 K, but many narrow bands are clearly visible at 80 K (Figure 5, S6, and S8). The number of expected modes is the same in this temperature range. Therefore, much smaller number of bands at 340 K than at 80 K can be attributed to band broadening that causes overlap of many bands. The significant increase in bandwidth of lattice modes when going from 80 to 340 K points to strong enhancement of thermal motions. It is worth adding that the lowest-wavenumber mode is observed at 24 cm^{-1} (80 K), whereas such a mode was observed at 37 cm^{-1} (77 K) for $FAPbCl_3$ and 42 cm^{-1} (100 K) for $MAPbCl_3$.[28,59] Thus, $MHyPbCl_3$ seems to be more soft than $MAPbCl_3$ and $FAPbCl_3$ and this behavior as well as shift of the lowest-wavenumber modes are related to change of the organic cation radius that decreases in the $MHy^+ > FA^+ > MA^+$ order.

https://dx.doi.org/10.1021/acs.jpcc.0c07886
J. Phys. Chem. C 2020, 124, 26999−27008

Raman spectra exhibit clear and abrupt changes when temperature changes from 340 to 345 K, indicating onset of the structural phase transition (Figures 5−7). This temperature interval is in a very good agreement with the DSC peak found at 342 K in the heating run.[25] In the high-wavenumber region, Raman bands do not show pronounced changes in intensities (Figures S5−S8) but many modes exhibit weak shifts, usually much below 4 cm^{-1} (Figures 6 and 7; Table S2). For instance, the $\rho(CH_3)$ modes exhibit upshifts (from 1091.1, 1113.4, and 1227.4 cm^{-1} at 340 K to 1094.7, 1114.5, and 1228.1 cm^{-1} at 345 K, Figures 6a,b and 7c), whereas the $\nu_{as}(CNN)$, $\delta(NH_2)$, and $\nu(NH_2)$ modes exhibit downshifts (from 1011.3, 1598.1, and 3223.7 cm^{-1} at 340 K to 1010.2, 1595.9, and 3222.2 cm^{-1} at 345 K, respectively; Figure 7a,d,f). These changes indicate that the phase transition affects HBs and structure of MHy^+. Furthermore, a number of doublets coalescence into singlets in the HT phase (Figures S5−S8). For example, this behavior is observed for the $\nu(NH_2)$ and $\nu_s(CH_3)$ modes (Figures S5, S7, and 6c,d). Another characteristic change is disappearance of many bands at 345 K. The smaller number of observed Raman bands in the HT phase is consistent with higher symmetry of this phase. According to X-ray diffraction data, the LT phase comprises two crystallographically unique MHy^+ cations[25] and according to the selection rules, they should give rise to four $\nu_s(CH_3)$ Raman bands (2A + 2B, Table S1). However, for very weak Davydov splitting, only two bands could be expected. We observe only two $\nu_s(CH_3)$ bands for the LT phase, in agreement with negligible Davydov splitting. In the HT phase, there is only one unique MHy^+ cation and in the polarization configuration used here, two $\nu_s(CH_3)$ bands should be observed ($A_1 + B_2$). Similarly to that in the LT phase, Davydov splitting is negligible and we observe only one band. Finally, the phase transition also leads to increase in FWHM values (Figures 6a,d and 7). However, these changes are small, just a few cm^{-1}, and much weaker than that observed previously for $MHyPbBr_3$, MHy_2PbI_4, or methylhydrazinium metal formates,[7,16,24] which transformed from ordered to disordered phases. Raman data confirm therefore that MHy^+ cations remain ordered in the HT phase.

The phase transition leads also to a few characteristic changes in the lattice modes region. First, some bands shift to lower or higher wavenumbers (Figure 5 and Table S2). For instance, the 98 cm^{-1} band at 340 K shifts to 92 cm^{-1} at 345 K (Figure 5a). Second, some bands coalescence or become narrower. This behavior is observed, for instance, for the 76 and 65 cm^{-1} bands (values at 80 K) that merge into one band at 66 cm^{-1} when temperature increases to 345 K (Figure 5a). Third, some bands exhibit significant change in intensity (see, for instance, the 46 cm^{-1} band in the $c(aa + ab)\bar{c}$ polarization; Figure 5b). The observed changes are consistent with the first-order character of the phase transition and increased symmetry of the HT phase. However, these changes are not very pronounced, indicating that the phase transition leads to relatively weak changes in the framework distortion and $PbCl_6$ tilts.

High-Pressure Raman Spectra. The Raman spectra of $MHyPbCl_3$ on compression are presented in Figure 8, and the pressure dependence of Raman wavenumbers is shown in Figure 9. The values of wavenumber intercepts at zero pressure (ω_0) and pressure coefficients ($\alpha = d\omega/dP$) obtained from fitting of the experimental data with a linear function $\omega(P) = \omega_0 + \alpha P$ are listed in Table S3.

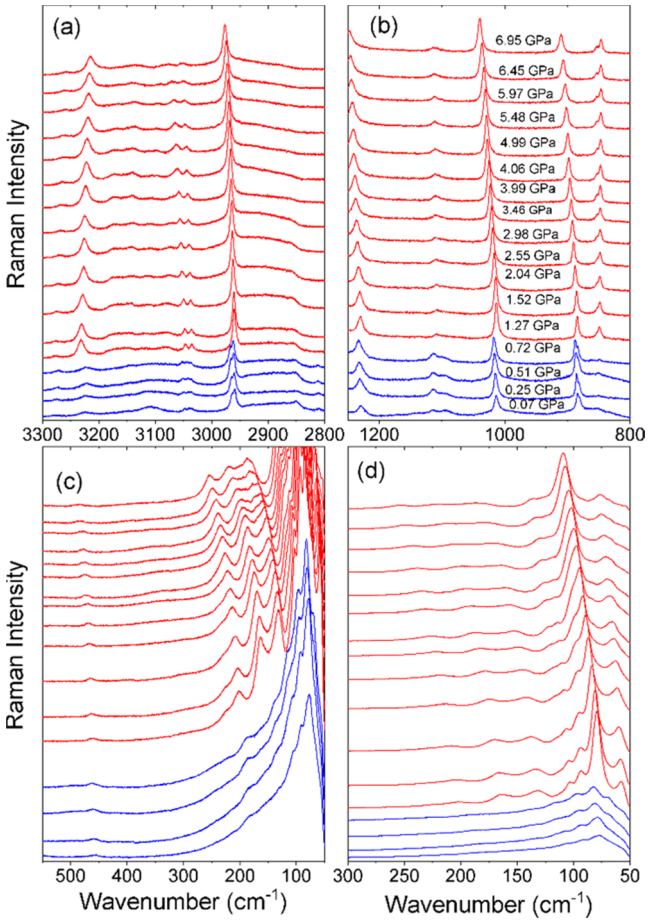

Figure 8. Raman spectra of $MHyPbCl_3$ for compression run.

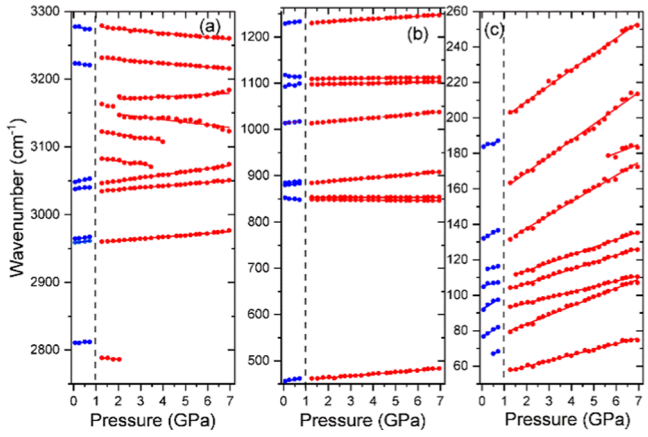

Figure 9. Pressure dependence of the Raman modes during the compression run. The solid lines are linear fits on the data to $\omega(P) = \omega_0 + \alpha P$. The vertical lines correspond to the phase-transition pressure.

The Raman spectra do not change qualitatively with increasing pressure up to 0.72 GPa. Table S3 shows that the $\nu(NH_2)$ and $\rho(NH_2)$ modes exhibit negative pressure dependence. This behavior indicates strengthening of the N−H···Cl HBs on compression. Similar behavior was reported for IR-active modes of $FAPbI_3$, but the pressure coefficients α are significantly smaller for $MHyPbCl_3$ (up to −6.53 cm^{-1} GPa^{-1}; see Table S3) than for $FAPbI_3$ (up to −15.4 cm^{-1} GPa^{-1}),[37] indicating a weaker effect of pressure on the HBs.

https://dx.doi.org/10.1021/acs.jpcc.0c07886
J. Phys. Chem. C 2020, 124, 26999−27008

The CNN and lattice modes of $MHyPbCl_3$ shift to higher wavenumbers on compression (Table S3). This behavior indicates that pressure leads to a significant compression of the C−N, N−N, and Pb−Cl bonds.

On further increase of pressure, Raman spectra exhibit a sudden change at 1.27 GPa (Figures 8 and 9). First, the cage modes exhibit large shifts and change in intensity. This behavior proves that the phase transition near 1 GPa is associated with change in the tilting and distortion of the $PbCl_6$ octahedral units. Thus, $MHyPbCl_3$ behaves in a similar way to the MA and FA analogues, for which the phase transitions observed below 1 GPa (for $MAPbX_3$ and $FAPbX_3$, X = I, Br) and at 2 GPa (for $MAPbCl_3$) were also attributed to tilts and distortion of the PbX_6 octahedra.[42−48] Second, the bands involving translational and librational motions of MHy^+ cations show a significant increase in intensity and narrowing (Figure 8c and Table S3). Since the MHy^+ cations are ordered in the ambient-pressure phase, such a behavior cannot be attributed to locking of these ions. Therefore, we attribute this behavior to decreased rotational degree of freedom of MHy^+ cations in the high-pressure phase. Third, the two N−H stretching modes observed at 3220.6 and 3273.5 cm^{-1} at 0.72 GPa shift to higher wavenumbers (3231.5 and 3279.0 cm^{-1}, respectively) at 1.27 GPa. A shift to higher wavenumber is also observed for the $\rho(NH_2)$ mode (847.9 cm^{-1} at 0.72 GPa). Furthermore, this mode splits at 1.27 GPa into 848.6 + 853.5 cm^{-1} doublet and its intensity strongly increases (Figures 8b and 9b). The observed upshifts and change in intensity point to a significant reconstruction of the HBs network and decrease of the HBs strength, probably due to significant reorientation of MHy^+ cations. Fourth, the $\nu_{as}(CNN)$ and $\nu_s(CNN)$ bands show jump-shifts to lower wavenumbers by up to 3.7 cm^{-1}. Very clear shifts to lower wavenumbers are also noted for all modes related to vibrations of CH_3 groups. This behavior confirms weakening of amine-framework interactions in the high-pressure phase. Moreover, the splitting observed in the ambient-pressure phase for the $\nu_s(CNN)$ mode near 880 cm^{-1} and the $\nu_s(CH_3)$ mode near 2960 cm^{-1} disappears in the high-pressure phase. This behavior resembles that observed in the transformation from the LT to HT phase at 345 K and could be probably attributed to the decrease of the crystallographically unique MHy^+ cations from two in the ambient phase to only one in the high-pressure phase.

On further increase of pressure, the spectra do not show any changes that could indicate onset of another phase transition. The $\nu(NH_2)$ bands show a negative pressure dependence, and nearly all other bands exhibit a positive pressure dependence, pointing to increasing amine-framework interactions and HBs strength on compression of this phase. Except the 200−100 cm^{-1} modes, nearly all other modes show significantly reduced pressure coefficients α, compared to the ambient-pressure phase (Table S3). This behavior points to the smaller compressibility of the high-pressure phase. Raman spectra also show that the bands remain narrow up to the highest pressure reached in our experiment (6.95 GPa). Thus, in contrast to the FA and MA analogues, there is no evidence of pressure-induced amorphization of $MHyPbCl_3$.

The Raman spectra of $MHyPbCl_3$ upon decompression show that the ambient-pressure phase is recovered (Figure S9), indicating reversibility of the phase transition.

CONCLUSIONS

^1H MAS NMR experiments demonstrated that the MHy^+ cations in $MHyPbCl_3$ are only weakly affected by the temperature-induced phase transition. This suggests a displacive type of the phase transition dominated by deformation of the $PbCl_6$ octahedra. ^{207}Pb MAS NMR measurements revealed two signals that correspond to two differently distorted $PbCl_6$ octahedra, namely, moderately distorted $Pb(1)Cl_6$ and significantly distorted $Pb(2)Cl_6$. Temperature-dependent measurements of the ^{207}Pb chemical shift tensor revealed a first-order character of the phase transition. These results also demonstrated that distortion of the $Pb(1)Cl_6$ octahedra becomes smaller on transition to the HT phase, whereas an opposite behavior is observed for the $Pb(2)Cl_6$ units

Raman studies revealed many similarities between the phonon properties of 3D methylhydrazinium lead halides and known MA and FA analogues. In particular, these families of compounds showed an increase of cage modes' wavenumbers when large I^- are replaced by smaller Br^- and then Cl^-. They also showed very pronounced sensitivity of the CH_3 torsional mode on halide type. Furthermore, in both the MHy and MA analogues, this torsional mode gives rise to a very broad Raman band, even at very low temperatures. These features indicate strong coupling of the molecular torsion with the cage. Temperature dependence of Raman spectra showed weak shifts and broadening at the phase-transition temperature for bands related to MHy^+ internal modes. Much more pronounced shifts and changes in bands' intensities were, however, observed for the lattice modes. Raman data confirm, therefore, that the phase transition in $MHyPbCl_3$ is not driven by temperature-induced unlocking of reorientational motions of the MHy^+ cations but by tilting and deformation of $PbCl_6$ octahedra, in agreement with the NMR results.

Pressure-dependent Raman studies revealed the onset of one pressure-induced phase transition between 0.72 and 1.27 GPa. The abrupt changes in the Raman spectra point to a first-order character of this transition. Analysis of the spectra indicates that the phase transition is associated with a change in the tilting and distortion of the $PbCl_6$ octahedral units. It is also accompanied by reorientation of MHy^+ cations. Thus, similarly to the MA and FA analogues, the driving force for the pressure-induced phase transition is tilting and distortion of the octahedral units. However, in contrast to the majority of MA and FA analogues, no evidence of a second phase transition or amorphization at higher pressures could be found for $MHyPbCl_3$.

ASSOCIATED CONTENT

Supporting Information

The Supporting Information is available free of charge at https://pubs.acs.org/doi/10.1021/acs.jpcc.0c07886.

Correlation diagram, Raman wavenumbers at different temperatures and assignment of modes, and wavenumber intercepts at zero pressure and pressure coefficients (Tables S1−S3) and temperature-dependent NMR and Raman spectra and high-pressure Raman spectra during decompression run (Figures S1−S9) (PDF)

https://dx.doi.org/10.1021/acs.jpcc.0c07886
J. Phys. Chem. C 2020, 124, 26999−27008

AUTHOR INFORMATION

Corresponding Author

Mirosław Mączka − *Institute of Low Temperature and Structure Research, Polish Academy of Sciences, 50-422 Wrocław, Poland;* orcid.org/0000-0003-2978-1093; Email: m.maczka@int.pan.wroc.pl

Authors

Maciej Ptak − *Institute of Low Temperature and Structure Research, Polish Academy of Sciences, 50-422 Wrocław, Poland;* orcid.org/0000-0002-4639-2367

Daniel Linhares Militão Vasconcelos − *Faculdade de Fisica, Universidade Federal do Ceara, 60455-970 Fortaleza, Brazil*

Laisvydas Giriunas − *Faculty of Physics, Vilnius University, LT-10222 Vilnius, Lithuania*

Paulo Tarso Cavalcante Freire − *Faculdade de Fisica, Universidade Federal do Ceara, 60455-970 Fortaleza, Brazil;* orcid.org/0000-0002-2321-3709

Marko Bertmer − *Felix Bloch Institute for Solid State Physics, Leipzig University, D-04103 Leipzig, Germany;* orcid.org/0000-0002-3208-7927

Juras Banys − *Faculty of Physics, Vilnius University, LT-10222 Vilnius, Lithuania*

Mantas Simenas − *Faculty of Physics, Vilnius University, LT-10222 Vilnius, Lithuania;* orcid.org/0000-0002-2733-2270

Complete contact information is available at: https://pubs.acs.org/10.1021/acs.jpcc.0c07886

Author Contributions

The manuscript was written through contributions of all authors. All authors have given approval to the final version of the manuscript.

Notes

The authors declare no competing financial interest.

ACKNOWLEDGMENTS

This research was supported by the National Science Center (Narodowe Centrum Nauki) in Poland under project no. 2019/35/B/ST5/00043 and by the Research Council of Lithuania (LMTLT), agreement no. S-MIP-19-4.

REFERENCES

(1) Li, W.; Wang, Z.; Deschler, F.; Gao, S.; Friend, R. H.; Cheetham, A. K. Chemically Diverse and Multifunctional Hybrid Organic-Inorganic Perovskites. *Nat. Rev. Mater.* **2017**, *2*, No. 16099.

(2) Saparov, B.; Mitzi, D. B. Organic-Inorganic Perovskites: Structural Versatility for Functional Materials Design. *Chem. Rev.* **2016**, *116*, 4558−4596.

(3) Jain, P.; Ramachandran, V.; Clark, R. J.; Zhou, H. D.; Toby, B. H.; Dalal, N. S.; Kroto, H. W.; Cheetham, A. K. Multiferroic Behavior Associated with an Order−Disorder Hydrogen Bonding Transition in Metal−Organic Frameworks (MOFs) with the Perovskite ABX_3 Architecture. *J. Am. Chem. Soc.* **2009**, *131*, 13625−13627.

(4) Tian, Y.; Stroppa, A.; Chai, Y.; Yan, L.; Wang, S.; Barone, P.; Picozzi, S.; Sun, Y. Cross Coupling Between Electric and Magnetic Orders in a Multiferroic Metal-Organic Framework. *Sci. Rep.* **2014**, *4*, No. 6062.

(5) Tian, Y.; Stroppa, A.; Chai, Y. S.; Barone, P.; Perez-Mato, M.; Picozzi, S.; Sun, Y. High-temperature Ferroelectricity and Strong Magnetoelectric Effects in a Hybrid Organic-Inorganic Perovskite Framework. *Phys. Status Solidi RRL* **2015**, *9*, 62−67.

(6) Gómez-Aguirre, L. C.; Pato-Doldán, B.; Mira, J.; Castro-García, S.; Señarís-Rodríguez, M. A.; Sánchez-Andújar, M.; Singleton, J.; Zapf, V. S. Magnetic-Ordering Induced Multiferroic Behavior in $[CH_3NH_3][Co(HCOO)_3]$ Metal-Organic Framework. *J. Am. Chem. Soc.* **2016**, *138*, 1122−1125.

(7) Mączka, M.; Gągor, A.; Ptak, M.; Paraguassu, W.; Da Silva, T. A.; Sieradzki, A.; Pikul, A. Phase Transitions and Coexistence of Magnetic and Electric Orders in the Methylhydrazinium Metal Formates. *Chem. Mater.* **2017**, *29*, 2264−2275.

(8) Bermúdez-Garcia, J. M.; Sánchez-Andújar, M.; Castro-García, S.; López-Beceiro, J.; Artiaga, R.; Señarís-Rodríguez, M. A. Giant Barocaloric Effect in the Ferroic Organic-Inorganic Hybrid $[TPrA][Mn(dca)_3]$ Perovskite Under Easily Accessible Pressures. *Nat. Commun.* **2017**, *8*, No. 15715.

(9) Mączka, M.; Gągor, A.; Ptak, M.; Stefańska, D.; Macalik, L.; Pikul, A.; Sieradzki, A. Structural, Phonon, Magnetic and Optical Properties of Novel Perovskite-like Frameworks of TriBuMe$[M(dca)_3]$ (TriBuMe = Tributylmethylammonium; dca = Dicyanamide; M = Mn^{2+},Fe^{2+}, Co^{2+}, Ni^{2+}). *Dalton Trans.* **2019**, *48*, 13006−13016.

(10) Zhao, M. M.; Zhou, L.; Shi, P. P.; Zheng, X.; Chen, X. G.; Gao, J. X.; Geng, F. J.; Ye, Q.; Fu, D. W. Halogen Substitution Effects on Optical and Electrical Properties in 3D Molecular Perovskites. *Chem. Commun.* **2018**, *54*, 13275−13278.

(11) Mączka, M.; Ptak, M.; Gągor, A.; Sieradzki, A.; Peksa, P.; Usevicius, G.; Simenas, M.; Furtado Leite, F.; Paraguassu, W. Temperature- and Pressure-Dependent Studies of a Highly Flexible and Compressible Perovskite-Like Cadmium Dicyanamide Framework Templated with Protonated Tetrapropylamine. *J. Mater. Chem. C* **2019**, *7*, 2408−2420.

(12) Qian, K.; Zhao, F.; Yan, Z.; Pang, J.; Chen, X.; Yang, C. A Perovskite-type Cage Compound As a Temperature-triggered Dielectric Switchable Material. *CrystEngComm* **2016**, *18*, 7671−7674.

(13) Trzebiatowska, M.; Gągor, A.; Macalik, L.; Peksa, P.; Sieradzki, A. Phase transition in the extreme: a cubic-to-triclinic symmetry change in dielectrically switchable cyanide perovskites. *Dalton Trans.* **2019**, *48*, 15830−15840.

(14) Smith, M. D.; Connor, B. A.; Karunadasa, H. I. Tuning the Luminescence of Layered Halide Perovskites. *Chem. Rev.* **2019**, *119*, 3104−3139.

(15) Maczka, M.; Ptak, M. Simple, Fast and Non-destructive Method for Detection of Dimethylammonium Impurity in Photovoltaic Methylammonium Lead Halides. *Appl. Solid State Chem.* **2019**, *3*, 45−48.

(16) Mączka, M.; Ptak, M.; Gągor, A.; Stefańska, D.; Sieradzki, A. Layered Lead Iodide of $[Methylhydrazinium]_2PbI_4$ with a Reduced Band Gap: Thermochromic Luminescence and Switchable Dielectric Properties Triggered by Structural Phase Transitions. *Chem. Mater.* **2019**, *31*, 8563−8575.

(17) Hoefler, S. F.; Trimmel, G.; Rath, T. Progress on Lead-Free Metal Halide Perovskites for Photovoltaic Applications: a Review. *Monatsh. Chem.* **2017**, *148*, 795−826.

(18) Wang, F.; Cao, Y.; Chen, C.; Chen, Q.; Wu, X.; Li, X.; Qin, T.; Huang, W. Materials Toward the Upscaling of Perovskite Solar Cells: Progress, Challenges, and Strategies. *Adv. Funct. Mater.* **2018**, *28*, No. 1803753.

(19) Quan, L. N.; Rand, B. P.; Friend, R. H.; Mhaisalkar, S. G.; Lee, T.-W.; Sargent, E. H. Perovskites for Next-Generation Optical Sources. *Chem. Rev.* **2019**, *119*, 7444−7477.

(20) Zhao, X.; Ng, J. D. A.; Friend, R. H.; Tan, Z.-K. Opportunities and Challenges in Perovskite Light-Emitting Devices. *ACS Photonics* **2018**, *5*, 3866−3875.

(21) Mykhaylyk, V. B.; Kraus, H.; Saliba, M. Bright and Fast Scintillation of Organolead Perovskite $MAPbBr_3$ at Low Temperatures. *Mater. Horiz.* **2019**, *6*, 1740−1747.

(22) Adinolfi, V.; Ouellette, O.; Saidaminov, M. I.; Walters, G.; Abdelhady, A. L.; Bakr, O. M.; Sargent, E. H. Fast and Sensitive Solution-Processed Visible-Blind Perovskite UV Photodetectors. *Adv. Mater.* **2016**, *28*, 7264−7268.

(23) Chen, W.; Bhaumik, S.; Veldhuis, S. A.; Xing, G.; Xu, Q.; Grätzel, M.; Mahaisalkar, S.; Mathews, N.; Sum, T. C. Giant Five-

Photon Absorption from Multidimensional Core-shell Halide Perovskite Colloidal Nanocrystals. *Nat. Commun.* **2017**, *8*, No. 15198.
(24) Mączka, M.; Ptak, M.; Gągor, A.; Stefańska, D.; Zaręba, J. K.; Sieradzki, A. Methylhydrazinium Lead Bromide: Noncentrosymmetric Three-Dimensional Perovskite with Exceptionally Large Framework Distortion and Green Photoluminescence. *Chem. Mater.* **2020**, *32*, 1667−1673.
(25) Mączka, M.; Gagor, A.; Zaręba, J. K.; Stefanska, D.; Drozd, M.; Balciunas, S.; Šimėnas, M.; Banys, J.; Sieradzki, A. Three-Dimensional Perovskite Methylhydrazinium Lead Chloride with Two Polar Phases and Unusual Second-Harmonic Generation Bistability above Room Temperature. *Chem. Mater.* **2020**, *32*, 4072−4082.
(26) Xu, W. J.; Du, Z. Y.; Zhang, W. X.; Chen, X. M. Structural Phase Transitions in Perovskite Compounds Based on Diatomic or Multiatomic Bridges. *CrysEngComm* **2016**, *18*, 7915−7928.
(27) Ibaceta-Jaña, J.; Muydinov, R.; Rosado, P.; Mirhosseini, H.; Chugh, M.; Nazarenko, O.; Dirin, D. N.; Heinrich, D.; Wagner, M. R.; Kühne, T. D.; et al. Vibrational Dynamics in Hybrid Lead Halide Perovskites Investigated by Raman Spectroscopy. *Phys. Chem. Chem. Phys.* **2020**, *22*, 5604−5614.
(28) Kontos, A. G.; Manolis, G. K.; Kaltzoglou, A.; Palles, D.; Kamitsos, E. I.; Kanatzidis, M. G.; Falaras, P. Halogen-NH_2^+ Interaction, Temperature-Induced Phase Transition, and Ordering in $(NH_2CHNH_2)PbX_3$ (X = Cl, Br, I) Hybrid Perovskites. *J. Phys. Chem. C* **2020**, *124*, 8479−8487.
(29) Odin, C. NMR studies of Phase Transitions. *Annu. Rep. NMR Spectrosc.* **2006**, *59*, 117−205.
(30) Besara, T.; Jain, P.; Dalal, N. S.; Kuhns, P. L.; Reyes, A. P.; Kroto, H. W.; Cheetham, A. K. Mechanism of the Order-Disorder Phase Transition, and Glassy Behavior in the Metal-Organic Framework $[(CH_3)_2NH_2]Zn(HCOO)_3$. *Proc. Natl. Acad. Sci. U.S.A.* **2011**, *108*, 6828−6832.
(31) Xu, J.; Lucier, B. E.; Sinelnikov, R.; Terskikh, V. V.; Staroverov, V. N.; Huang, Y. Monitoring and Understanding the Paraelectric-Ferroelectric Phase Transition in the Metal-Organic Framework $[NH_4][M(HCOO)_3]$ by Solid-State NMR Spectroscopy. *Chem. − Eur. J.* **2015**, *21*, 14348−14361.
(32) Asaji, T.; Yoshitake, S.; Ito, Y.; Fujimori, H. Phase Transition and Cationic Motion in the Perovskite Formate Framework $[(CH_3)_2NH_2][Mg(HCOO)_3]$. *J. Mol. Struct.* **2014**, *1076*, 719−723.
(33) Armstrong, R. L.; Lourens, J. A. J.; Stroud, J. D. ^{133}Cs Spin-Lattice Relaxation Study of Phase Transitions in $CsPbCl_3$. *Phys. Rev. B* **1976**, *13*, 5099−5101.
(34) Sharma, S.; Weiden, N.; Weiss, A. ^{207}Pb and ^{205}Tl NMR on Perovskite Type Crystals $APbX_3$ (A= Cs, Tl, X= Br, I). *Z. Naturforsch., A: Astrophys., Phys. Phys. Chem.* **1987**, *42*, 1313−1320.
(35) Xu, Q.; Eguchi, T.; Nakayama, H.; Nakamura, N.; Kishita, M. Molecular Motions and Phase Transitions in Solid $CH_3NH_3PbX_3$ (X= C1, Br, I) as Studied by NMR and NQR. *Z. Naturforsch., A: Astrophys., Phys. Phys. Chem.* **1991**, *46*, 240−246.
(36) Ran Lim, A.; Kim, I. G. Phase Transition Study by Using ^{133}Cs and ^{207}Pb Nuclear Magnetic Resonance in a $CsPbCl_3$ Single Crystal. *J. Phys. Soc. Jpn.* **2004**, *73*, 475−479.
(37) Franssen, W. M.; Van Es, S. G.; Dervişoğlu, R.; De Wijs, G. A.; Kentgens, A. P. Symmetry, Dynamics, and Defects in Methylammonium Lead Halide Perovskites. *J. Phys. Chem. Lett.* **2017**, *8*, 61−66.
(38) Baikie, T.; Barrow, N. S.; Fang, Y.; Keenan, P. J.; Slater, P. R.; Piltz, R. O.; Gutmann, M.; Mhaisalkar, S. G.; White, T. J. A Combined Single Crystal Neutron/X-ray Diffraction and Solid-State Nuclear Magnetic Resonance Study of the Hybrid Perovskites $CH_3NH_3PbX_3$ (X = I, Br and Cl). *J. Mater. Chem. A* **2015**, *3*, 9298−9307.
(39) Senocrate, A.; Moudrakovski, I.; Maier, J. Short-Range Ion Dynamics in Methylammonium Lead Iodide by Multinuclear Solid State NMR and ^{127}I NQR. *Phys. Chem. Chem. Phys.* **2018**, *20*, 20043−20055.
(40) Bernard, G. M.; Wasylishen, R. E.; Ratcliffe, C. I.; Terskikh, V.; Wu, Q.; Buriak, J. M.; Hauger, T. Methylammonium Cation Dynamics in Methylammonium Lead Halide Perovskites: A Solid-State NMR Perspective. *J. Phys. Chem. A* **2018**, *122*, 1560−1573.
(41) Furukawa, Y.; Nakamura, D. Cationic Dynamics in the Crystalline Phases of $(CH_3NH_3)PbX_3$ (X: Cl, Br) as Studied by Proton Magnetic Resonance Techniques. *Z. Naturforsch., A: Astrophys., Phys. Phys. Chem.* **1989**, *44*, 1122−1126.
(42) Swainson, I. P.; Tucker, M. G.; Wilson, D. J.; Winkler, B.; Milman, V. Pressure Response of an Organic-Inorganic Perovskite: Methylammonium Lead Bromide. *Chem. Mater.* **2007**, *19*, 2401−2405.
(43) Jaffe, A.; Lin, Y.; Beavers, C. M.; Voss, J.; Mao, W. L.; Karunadasa, H. I. High-Pressure Single-Crystal Structures of 3D Lead Halide Hybrid Perovskites and Pressure Effects on Their Electronic and Optical Properties. *ACS Cent. Sci.* **2016**, *2*, 201−209.
(44) Szafrański, M.; Katrusiak, A. Mechanism of Pressure-induced, Phase Transitions, Amorphization, and Absorption-edge Shift in Photovoltaic Methylammonium Lead Iodide. *J. Phys. Chem. Lett.* **2016**, *7*, 3458−3466.
(45) Francisco-López, A.; Charles, B.; Weber, O. J.; Alonso, M. I.; Garriga, M.; Campoy-Quiles, M.; Weller, M. T.; Goni, A. R. Pressure Induced Locking of Methylammonium Cations Versus Amorphization in Hybrid Lead Iodide Perovskites. *J. Phys. Chem. C* **2018**, *122*, 22073−22082.
(46) Wang, L.; Wang, K.; Xiao, G.; Zeng, Q.; Zou, B. Pressure Induced Structural Evolution and Band Gap Shifts of Organometal Halide Perovskite-based Methylammonium Lead Chloride. *J. Phys. Chem. Lett.* **2016**, *7*, 5273−5279.
(47) Wang, L.; Wang, K.; Zou, B. Pressure-Induced Structural and Optical Properties of Organometal Halide Perovskite-Based Formamidinium Lead Bromide. *J. Phys. Chem. Lett.* **2016**, *7*, 2556−2562.
(48) Wang, P.; Guang, J.; Galeschuk, D. T. K.; Yao, Y.; He, C. F.; Jiang, S.; Zhang, S.; Liu, Y.; Jin, M.; Jin, C. Y.; et al. Pressure-Induced Polymorphic, Optical, and Electronic Transitions of Formamidinium Lead Iodide Perovskite. *J. Phys. Chem. Lett.* **2017**, *8*, 2119−2125.
(49) Jiang, S.; Luan, Y.; Jang, J. I.; Baikie, T.; Huang, X.; Li, R.; Saouma, F. O.; Wang, Z.; White, T. J.; Fang, J. Phase Transitions and Formamidinium Lead IodidePerovskite under Pressure. *J. Am. Chem. Soc.* **2018**, *140*, 13952−13957.
(50) Wang, H.; Zhao, M.; Ackerman, J. L.; Song, Y. Saturation-inversion-recovery: A method for T1 measurement. *J. Magn. Res.* **2017**, *274*, 137−143.
(51) Maciel, G. E.; Dallas, J. L. ^{207}Pb pulse Fourier Transform Nuclear Magnetic Resonance. Promising New Tool for Studies in Lead Chemistry. *J. Am. Chem. Soc.* **1973**, *95*, 3039−3040.
(52) Massiot, D.; Fayon, F.; Capron, M.; King, I.; Le Calve, S.; Alonso, B.; Durand, J.-O.; Bujoli, B.; Gan, Z.; Hoatson, G. Modelling One- and Two-Dimensional Solid-State NMR Spectra. *Magn. Reson. Chem.* **2002**, *40*, 70−76.
(53) Bio-Rad Laboratories, Inc. SpectraBase, 2020. Available: https://spectrabase.com/spectrum/5Y1wPESgfC5. June 11, 2020.
(54) Karmakar, A.; Askar, A. M.; Bernard, G. M.; Terskikh, V. V.; Ha, M.; Patel, S.; Shankar, K.; Michaelis, V. K. Mechanochemical Synthesis of Methylammonium Lead Mixed-Halide Perovskites: Unraveling the Solid-Solution Behavior Using Solid-State NMR. *Chem. Mater.* **2018**, *30*, 2309−2321.
(55) Bernard, G. M.; Goyal, A.; Miskolzie, M.; McKay, R.; Wu, Q.; Wasylishen, R. E.; Michaelis, V. K. Methylammonium Lead Chloride: A Sensitive Sample for an Accurate NMR Thermometer. *J. Magn. Res.* **2017**, *283*, 14−21.
(56) Alexandrov, K.; Besnosikov, B.; Posdnjakova, L. Successive Phase Transitions in Perovskites. II. Structures of Distorted Phases. *Ferroelectrics* **1976**, *12*, 197−198.
(57) Bernasconi, A.; Page, K.; Dai, Z.; Tan, L. Z.; Rappe, A. M.; Malavasi, L. Ubiquitous Short-Range Distortion of Hybrid Perovskites and Hydrogen-Bonding Role: the $MAPbCl_3$ Case. *J. Phys. Chem. C* **2018**, *122*, 28265−28272.
(58) Mason, J. Conventions for the Reporting of Nuclear Magnetic Shielding (or Shift) Tensors Suggested by Participants in the NATO ARW on NMR Shielding Constants at the University of Maryland,

College Park, July 1992. *Solid State Nucl. Magn. Reson.* **1993**, *2*, 285−288.
(59) Leguy, A. M. A.; Goñi, A. R.; Frost, J. M.; Skelton, J.; Brivio, F.; Rodriguez-Martinez, X.; Weber, O. J.; Pallipurath, A.; Alonso, M. I.; Campoy-Quiles, M.; Weller, M. T.; et al. Dynamic Disorder, Phonon Lifetimes, and the Assignment of Modes to the Vibrational Spectra of Methylammonium Lead Halide Perovskites. *Phys. Chem. Chem. Phys.* **2016**, *18*, 27051−27066.
(60) Durig, J. R.; Harris, W. C.; Wertz, D. W. Infrared and Raman Spectra of Substituted Hydrazines. I. Methylhydrazine. *J. Chem. Phys.* **1969**, *50*, 1449−1461.

https://dx.doi.org/10.1021/acs.jpcc.0c07886
J. Phys. Chem. C 2020, 124, 26999−27008